

Investigation of silicon-on-insulator CMOS integrated thermocouple and heater for antenna-coupled bolometer

メタデータ	言語: eng 出版者: 公開日: 2019-07-16 キーワード (Ja): キーワード (En): 作成者: Elamaran, Durgadevi, Satoh, Hiroaki, Hiromoto, Norihisa, Inokawa, Hiroshi メールアドレス: 所属:
URL	http://hdl.handle.net/10297/00026717

Investigation of silicon-on-insulator CMOS integrated thermocouple and heater for antenna-coupled bolometer

Durgadevi Elamaram¹, Hiroaki Satoh², Norihisa Hiromoto¹ and Hiroshi Inokawa^{1,2*}

¹*Graduate School of Science and Technology, Shizuoka University, Hamamatsu, Japan.*

²*Research Institute of Electronics, Shizuoka University, Hamamatsu, Japan.*

*E-mail: inokawa.hiroshi@shizuoka.ac.jp

Abstract

This paper presents the characterization of 0.6 μm silicon-on-insulator CMOS processed integrated thermocouple-heater device for bolometer applications. Two different kinds of thermocouple with poly- and single-crystalline silicon wires have been fabricated and the performances were evaluated in terms of responsivity (R_v) and noise equivalent power (NEP). Relatively large responsivity of 336 V/W and small noise equivalent power of $162 \text{ pW}/\sqrt{\text{Hz}}$ were obtained from the electrical characterization of 100- μm -long device. The high Seebeck coefficient of 346 $\mu\text{V/K}$ and the reduced thermal conductivity of 27.3 W/mK were obtained by the fabricated devices. Assuming the use in antenna-coupled bolometers to detect the wave at 1 THz, the thermocouple-heater device was adapted for a half-wave dipole antenna, and the performances were estimated and compared with those of other temperature sensors. Comparison revealed that the thermocouple-based bolometers showed competitive NEP and uniquely featured low power consumption.

1. Introduction

Recent thermal detector technology combined with semiconductor process technology, developed for integrated circuit technology have availed more exciting possibilities for the development of thermal radiation detector.¹⁾ Terahertz technology deals with the frequency region from 300 GHz to 3 THz have gained much attention due to the increased demand in military, surveillance, material identification and medical imaging.^{2,3)} Terahertz (THz) waves are non-ionizing, not harmful due to its low photon energy, and also enable high resolution images than far-infrared and millimeter waves, hence they can be applicable to bio-medical screening, diagnosis and imaging. Electromagnetic wave around 1 THz is of great interest for non-invasive and non-destructive imaging. The wide scope of THz technology enhances the development of highly sensitive, cost-effective and room-temperature operable THz detectors. THz detectors are mainly classified into photon detectors and thermal detectors.

Photon detectors operated near mid-infrared or lower frequency range has constraint from the small energy of photons resulting in additional cryogenic cooling system. In contrast, thermal detectors can operate at room temperature, and provide modest sensitivity and video-rate response if internal thermal conductance is in the order of 10^{-8} W/K and heat capacitance of the temperature sensor is in the order of 10^{-9} J/K.⁴⁾ Therefore, thermal detectors (bolometers) are applicable to THz imaging. Moreover, thermal detectors have the important advantages of reliability, cost-effective and room-temperature operation, which making it attractive for THz applications. Generally, in thermal detectors, radiated signal is detected as a change in material's property caused by the small temperature rise, consists of an absorber and temperature sensor.^{5, 6)} For longer wavelength, especially in THz region, the absorber size should be sufficiently large to circumvent diffraction limit by making its size more than λ/n_e for the electromagnetic wavelength (λ) and effective refractive index (n_e).⁷⁾ With such large absorber/sensor, it is difficult to get reduced thermal conductance and low heat capacity. Antenna-coupled bolometer was then addressed to resolve this problem, which has the ability to absorb THz power at low frequencies. Antenna-coupled microbolometer has been extensively studied from past three decades in which the radiation is absorbed by an antenna and converted to heat by a heater.

Another most important element in bolometer is the temperature sensor, and many kinds of

sensors, such as resistor (thermistor), pn-junction diode, FET, thermocouple, etc. are available. Conventional absorber type microbolometers- used wide variety of thermistor (resistor) materials such as vanadium-oxide,⁸⁻¹¹⁾ metal¹²⁻¹⁴⁾ and semi-conductors.^{15, 16)} For this kind of temperature sensor, temperature coefficient of resistance is vital parameter which improves the gain and noise of the detector. In case of semiconducting material, although it has very low TCR, it is very much compatible with the CMOS integration. In recent days, suspended field-effect transistor and diode based thermal sensors have been extensively pursued for THz and infrared detection.¹⁷⁻²³⁾ Recently thermocouple based infrared detector was reported by *Timofeev et al.*²⁴⁾, in which heavily doped silicon was used for thermocouple fabrication.

Thermocouple generally consists of two dissimilar metals or semiconducting materials joined at the point of temperature measurement, and other electrical junctions are formed at a reference temperature. Compared to ordinary metal or semiconducting materials, silicon (Si) is promising, since the use of Si integrated-circuit technology offers several advantages, such as excellent manufacturability, ease of down scaling for higher performance, possibility of integration with readout circuits, etc. Furthermore, a larger Seebeck effect is generally found in semiconducting materials including Si, which makes it an attractive material for thermocouple-based bolometers.²⁵⁾ In contrast to bulk Si, Si nanowires or nanostructures have gained much attention due to its low thermal conductivity and large Seebeck coefficient.²⁶⁾

In this work, thermocouples of heavily doped n⁺ and p⁺ single crystalline Si wires (Device A), and n⁺ polycrystalline and p⁺ single crystalline Si wires (Device B) have been characterized as a temperature sensor with n⁺ polycrystalline Si heater. In contrast to single crystalline silicon, polysilicon consists of individual grains. The phonons are scattered by the grain boundaries, which reduces the thermal conductivity as a result of reduced phonon mean path.^{27, 28)} The improved responsivity can be expected for the polycrystalline device since the reduced thermal conductance results in a larger temperature rise for an input power. In order to verify this expectation, two different kinds of devices made of single and polycrystalline silicon were compared. The purpose of this paper is to quantitatively clarify the usefulness of the thermocouple as a temperature sensor for the 1-THz antenna-coupled bolometer, in comparison with other bolometers utilizing different kinds of temperature

sensors such as FET, pn-junction diode and resistors. All the bolometers were fabricated by the 0.6 μm silicon-on-insulator (SOI) CMOS process technology without any introduction of non-standard materials such as VO_x , BiTe, PbTe, etc. Current work is the detailed description of our recent research report,²⁹⁾ which includes the comprehensive explanation of device design, experimental methods and extraction procedure of electrical and thermal parameters. And this time we also analyzed and compared the performance of thermocouple sensor with other temperature sensors fabricated by the same 0.6 μm SOI CMOS technology for the application in antenna-coupled bolometer. To the best of our knowledge, the SOI thermocouple has not yet been investigated as a temperature sensor for antenna-coupled THz bolometer.

2. Device Structure and Characterization Methods

The bolometer of this work was fabricated using a 0.6 μm CMOS-SOI process with additional local field oxide removal by CHF_3 reactive ion etching and cavity formation in Si substrate by SF_6 plasma etching for thermal isolation. Thicknesses of the buried oxide, SOI, polysilicon and gate oxide are 400, 100, 130 and 7 nm, respectively. The bolometer under study consists of a polysilicon heater, a Si dioxide interlayer and a thermocouple (combination of n- and p-type semiconducting materials) on a Si substrate. Figure 1 shows the schematic and cross-sectional diagrams of the bolometer in which the heater is made of phosphorous-doped polycrystalline Si with a width of 1 μm and a length of 100 μm , and two kinds of thermocouples with different combination of n- and p-type materials as shown in Table I. Heavily doped single crystalline Si with arsenic or boron is connected with a metal layer at the center to form the thermocouple of device A. Similarly, phosphorous-doped polycrystalline Si and boron-doped single crystalline Si forms the thermocouple of device B. The width and length of the thermocouple are the same as those of the heater. The optical micrograph and the field emission scanning electron microscopy (FE-SEM) images of the fabricated device are shown in Fig. 2.

The electrical measurements of the fabricated bolometers were carried out using low-temperature prober Nagase Techno-Engineering Grail 21-205-6-LV-R equipped with Keysight 4156C precision semiconductor parameter analyzer. Temperature coefficient of resistance (TCR) of polycrystalline heater was measured from the slope of resistance vs.

temperature in the temperatures range from 260 to 300 K. The sample temperature was controlled with an accuracy of ± 0.2 K by the Cryogenic Control Systems Inc. Cryocon 32 temperature controller installed in the prober. Responsivity was measured by applying AC input power up to $8 \mu\text{W}$ to the heater at a frequency of 10 Hz. Thermocouple output voltage was detected using Signal Recovery 7270 lock-in amplifier under nil bias current. Noise characteristics of thermocouple was evaluated using the low-temperature prober with Keysight 35670A FFT dynamic signal analyzer. DL Instruments 1201 low-noise voltage preamplifier was used to amplify the noise signal. The noise spectrum was recorded over the frequency range from 1 Hz to 100 kHz.

For the application of 1-THz antenna-coupled bolometer, the integrated thermocouple-heater device should be modified according to the structure shown in Fig. 3. This is based on the requirement that the thermocouple-heater device is located at the center of the half-wave dipole antenna, and should be sufficiently shorter than the total length of the antenna, i.e. $50 \mu\text{m}$. Note that this length is reduced from the half wavelength in the free space due to the presence of the substrate with a high dielectric constant.³⁰⁾ We also intended to compare the performance of the proposed device with those of other bolometers with different temperature sensors as shown later in Sect. 3. In order to set the common basis of comparison, the device length is set to $15 \mu\text{m}$. The width of the thermocouple is reduced to $0.6 \mu\text{m}$ to minimize the thermal conduction and realize a larger temperature rise since the minimum feature size of CMOS fabrication technology used this time is $0.6 \mu\text{m}$. The dimensions of the heater are also commonly set because the main subject of this research is to evaluate the thermocouple as a temperature sensor for the antenna-coupled bolometer. Based on this structure, the performance metrics such as responsivity (R_v) and noise equivalent power (NEP) has been estimated and compared with those of other temperature sensors.

3. Results and discussion

To estimate the thermal resistance and the temperature distribution along the composite wire consisting of the thermocouple, n^+ polysilicon heater, TCR and sheet resistance of the n^+ polysilicon layer have been measured at different temperatures, and is represented in Figs. 4 (a) and (b). Measured TCRs at 300 K for devices A and B are 0.114 and 0.112 %/K, respectively, and regarded the same within the accuracy of the measurement. For the purpose

of comparison, TCR of n⁺ and p⁺ single crystalline Si materials was also obtained from the devices fabricated on the same chip, which are 0.156 %/K and 0.104 %/K, respectively.

Temperature distribution along the suspended n⁺ polysilicon heater line (composite wire) has been estimated analytically based on the method described in Ref. 31) and 32), and is shown in Fig. 5(a) and (b). The normalized resistance increases with the square of the input current, based on this phenomenon the thermal resistance of the heater line was evaluated. The maximum range of heater current is limited to 50 μA since our aim is to evaluate the performance in few 10's of K without damaging the device. When an input current is dissipated at the heater, the temperature is increased at the center of the wire by ΔT with respect to the substrate temperature. The temperature rise (ΔT) of around 22 K at the center was obtained for both heaters at the maximum input current limit of 50 μA. The temperature rise (ΔT) also linearly increases with the square of the input current, which is represented in Fig. 6 (a). The total Seebeck coefficient *S* of fabricated thermocouple was determined by exciting an alternating input current at the heater. The developed open circuit voltage (ΔV) between two ends was observed by lock-in techniques at frequency of 10 Hz. The temperature rise (ΔT) is proportional to the applied input power, which is correlated with the measured open circuit voltage to find the Seebeck coefficient *S*. *S* can be written as,

$S = \frac{\Delta V}{\Delta T}$ usually represented in μV/K. The obtained Seebeck coefficients of device A and device B are 345 μV/K and 327 μV/K, respectively is shown in Fig. 6 (b).

Expected Seebeck coefficient *S* was predicted from the relationship between the carrier concentration and resistivity of n⁺, p⁺ single crystalline Si and n⁺ polycrystalline Si. The resistivities and estimated dopant concentrations³³⁾ are 0.97 mΩcm and 1 x 10²⁰ /cm³, 4.19 mΩcm and 2.5 x 10¹⁹ /cm³, and 0.92 mΩcm and >10²⁰ /cm³ for n⁺, p⁺ single crystalline Si and n⁺ polycrystalline Si, respectively. The measured Seebeck coefficients were compared with the previously reported values as shown in Table II. Generally speaking, the Seebeck coefficient depends on the dopant concentration, and shows larger values at lower concentrations. Therefore, direct comparison can be made only with the sum of absolute values from Ref. 34, i.e. |-190|+|375| μV/K, which is nearly 1.5 times larger than the values obtained in this work. The reduction of the obtained Seebeck coefficient may be due to the thickness effect as can be seen in the values from Ref. 24 for 40-nm film, which are relatively

small if the reduced dopant concentration is taken into account.

The thermal conductivity of material was then extracted from its corresponding thermal resistances (r_t), width (w) and thickness (t) is shown in equation (1). Thermal conductivity (k) of polysilicon was evaluated from the test structure fabricated on the same chip, consists of polysilicon wire and SiO₂ interlayer. The thermal conductivity of SiO₂ taken from Ref. 37 was used to eliminate its effect from the test structure. Since the separate test structures of n⁺ and p⁺ single crystalline silicon is unavailable the combined thermal conductivity was measured from its thermal resistance and the SiO₂ contribution was eliminated. It is to be noted that for 100 nm single crystalline Si the thermal conductivity is 27.4 W/mK, which is reduced approximately to the one fifth of the bulk value as a result of large dopant concentration and small thickness.

$$r_t = \frac{1}{k \times w \times t} \quad (1)$$

Electrical responsivity (R_v) is an important performance metrics for optimizing and designing the bolometer as the optical responsivity is proportional to the electrical responsivity, current work deals with the electrical characterization for the optimization of fabricated thermocouple design. Responsivity is a measure of developed output voltage due to the excitation of input power. To measure the responsivity of fabricated thermocouple, root mean square (*r.m.s*) input power was applied at the heater and the corresponding *r.m.s* output voltage at the thermocouple was observed using lock-in at 10 Hz and at 300 K. The slope of the output voltage versus input power gives the responsivity value. Fig. 7 (a) shows the measured electrical responsivity of the fabricated bolometer, it is found that device A shows slightly larger response than device B Since the responsivity (R_v) of thermocouple is proportional to the Seebeck coefficient ($R_v \propto S$), slightly large S improved the responsivity of device A. In detail the open circuit output voltage of thermocouple can be written as, $V_0 = \Delta T \times S$, where temperature rise is proportional to the input power and inverse of total thermal conductance ($\Delta T \propto \frac{P_{in}}{G_{th}}$). Then the responsivity of thermocouple can be modelled as,

$$V_0 \propto \frac{S \cdot I^2 \cdot R_h}{G_{th}} \quad (2)$$

$$\text{Responsivity} \propto \frac{S}{G_{th}} \quad (3)$$

Where I is the heater input current and R_h is the measured heater resistance. It is evident

that the responsivity can be made higher by improving the Seebeck coefficient and reducing the total thermal conductance. In comparison between two kinds of fabricated devices, larger responsivity of 336 V/W was obtained by device A. It is to be noted that the bias current is not needed to develop the voltage across the two ends of the thermocouple while in other temperature sensors bias current must be applied which leads to large power consumption. Fig. 7 (b) represents the heater input and output voltage response, since the same polysilicon heater with identical length is used for both the devices, the obtained ratio is almost close to each other. From the measured responsivity and the Seebeck coefficient the effective total thermal conductance can be calculated by $G_{th} = SR_v^{-1}$, and the total thermal conductance of device A and B are 1.03 $\mu\text{W/K}$ and 1.05 $\mu\text{W/K}$, respectively.

To check the cut off frequency (f_c) of fabricated bolometer, frequency response characteristics shown in Fig. 7 (c) was measured by applying input power of 1.5 μW at the heater. Fit line was drawn on the measured frequency response to find out the cut off frequency, which is 184 Hz and 191 Hz for device A and device B, respectively. Lower cut-off is probably due to the long length (L) of the bolometer, as cut-off frequency is inversely proportional to the square of length ($f_c \propto \frac{1}{L^2}$). Also there is a trade-off existing between the cut-off frequency and responsivity, responsivity could be further improved, if slower response is acceptable.

In order to determine NEP, noise measurement was performed on the fabricated thermocouples, which are represented in Fig. 7 (d). Numerical FFT was performed on the time-stamped voltage noise to get the output voltage noise power spectrum. To avoid over riding of spectrum analyzer, input to the thermocouple was AC coupled and the output was averaged to get better noise level. Noise power is generally proportional to the resistance of the device, where the thermocouple resistances of device A and device B are 28.6 k Ω and 27.4 k Ω , respectively. The dotted horizontal base lines shown in Fig. 7 (d) correspond to the theoretical Johnson noise based on the expression $V_n = \sqrt{4kTR}$ at 300 K. Measured voltage noise is almost close to the expected noise and spikes in the measured spectrum are due to the environmental noise. NEP, which is in inverse proportion to responsivity and direct proportion to voltage noise, was calculated based on the measured voltage noise at 10 Hz. The NEPs for the devices A and B are 162 $\text{pW}/\sqrt{\text{Hz}}$ and 228 $\text{pW}/\sqrt{\text{Hz}}$, respectively. The worse (larger) NEP for device B is caused by 1.27 times larger noise and 1.08 times

smaller responsivity. In general, the polysilicon resistor shows a larger low-frequency noise due to the carrier mobility fluctuation caused by the presence of grain boundaries.³⁸⁾ This might be the cause of the larger noise in device B. Further improvement in NEP could be possible, if the noise is reduced and/or responsivity is increased by the modification of material characteristics.

Our main intension is to apply the thermocouple device in the optimized antenna-coupled bolometer design for detecting 1-THz waves. For that purpose, the device structure was assumed as shown in Fig. 3 and then the measured characteristics were converted to the assumed device structure. To accommodate the thermocouple bolometer in the optimized design structure, the bolometer area must be minimized to 15 μm x 15 μm . Following assumptions have been made on the fabricated device characteristics to estimate the responsivity and noise. (1) Resistance (R) is proportional to the device length (L), R will reduce if the device length shrinks. (2) Thermal resistance ($R_t = r_t \times L$) is proportional to length L . (3) Temperature rise (ΔT) is proportional to length L .

I-V characteristics of the fabricated heater and thermocouple was converted to assumed heater and thermocouple by assuming constant resistivity between the fabricated and the assumed devices, and the heater resistance of assumed devices can be written as,

$$R_{hA} = R_{hF} \times \frac{15}{100} \quad (4)$$

Subscripts A and F represents the assumed and fabricated devices, respectively. Based on this ratio, the heater resistance and thermocouple resistance was estimated for the assumed structure. The temperature distribution of assumed device was then estimated from the converted heater resistance (R_{hA}) and thermal resistance(r_{tA}). The total thermal resistance (r_t) which has the contribution of polysilicon, single crystalline Si and SiO₂ was evaluated based on the thermal conductivity shown in Table III. Maximum temperature rise obtained for assumed devices A and B at 50 μA of heater input current are 0.55 K and 0.53 K. According to the equation (2) generated output voltage at the thermocouple is proportional to the temperature rise and Seebeck coefficient, since S does not have any relationship with length same value was utilized for the estimation of output voltage.

$$V_{0A} = \Delta T_A \times S \quad (5)$$

Responsivity which is also proportional to length was estimated for the assumed device,

which can be modelled as,

$$R_{vA} \propto \frac{15}{100} \times \frac{r_{tF}}{r_{tA}} \times R_{vF} \quad (6)$$

Estimated responsivity for the assumed devices A and B are 56.3 V/W and 49.3 V/W, respectively. It is clearly evident that responsivity is proportional to the device resistance and thermal resistance. Responsivity could be further improved by narrowing the Si layer as a result of the size effect in thermal conductivity.

Similarly, noise characteristics was also estimated for the assumed devices. The square of noise power spectral density is proportional to the device resistance, based on this the noise characteristics was estimated as,

$$\overline{V_{nA}^2} = \overline{V_{nF}^2} \times \frac{R_{tA}}{R_{tF}} \quad (7)$$

$$R_{tA} = R_{tF} \times \frac{15 \mu m}{100 \mu m} \times \frac{1 \mu m}{0.6 \mu m} \quad (8)$$

Since the noise voltage is proportional to the square root of resistance, it is decreased with the resistance. However, decreasing the resistance will affect the responsivity, hence a trade-off exists between the responsivity and noise. NEP are then calculated from the estimated voltage noise and responsivity, which are 483 pW/ \sqrt{Hz} and 702 pW/ \sqrt{Hz} for devices A and B, respectively.

In addition to that, the performance metrics of the current thermocouple sensor was compared with different temperature sensors such as FET, pn-junction diode and resistors, which were also fabricated by the same 0.6 μm CMOS-SOI process.³⁹⁾ Table IV represents the comparison results of different temperature sensors. FET based bolometer shows very large responsivity and better NEP due to its large amplification factor. But still the thermocouple based bolometer shows better NEP which is very close to FET based bolometer, even though its responsivity is two order magnitude lesser than that of FET, better NEP may be the cause of absence of bias current. Hence it can be concluded that the thermocouple based temperature sensors could be a good thermal detector for THz applications with further optimization.

4. Summary

The intention of this current study is to understand the behavior of thermocouple with heater as a bolometer by analyzing its important performance metrics such as responsivity and NEP

and to investigate its application in optimized antenna-coupled bolometer structure for detecting 1-THz waves. For this study, two different kinds of thermocouple devices had been fabricated with standard 0.6 μm CMOS-SOI without an introduction of toxic material, making it highly attractive for the integration with CMOS read-out circuits. The largest responsivity and better NEP of 336 V/W and 162 $\text{pW}/\sqrt{\text{Hz}}$ was obtained for the devices with p+ and n+ single crystalline Si thermocouple. The electrical responsivity results of bolometer is expected to reflect on optical responsivity of antenna-coupled bolometer. The application of thermocouple in antenna-coupled bolometer was investigated by changing its device dimension to the optimized device dimension. Responsivity and noise performances were estimated for the antenna-coupled devices, decreased responsivity in proportion with length was observed, as in *Tiwari, et al.*⁴⁰⁾ But, the noise characteristics were not much affected due to the absence of bias current. The results were compared with different temperature sensors fabricated by same SOI process. FET based bolometer shows good responsivity and NEP. Interestingly, the thermocouple based bolometer shows smaller noise voltage than FET based bolometer. Though it has very good noise voltage, the calculated NEP is larger than FET-based bolometer because of its poor responsivity. Further optimization of thermocouple-based bolometer by narrowing or using thin Si layer could improve the responsivity as a result of reduced thermal conductivity.⁴¹⁾ Hence, the thermocouple based bolometer could be a suitable detector for the application in antenna-coupled bolometer design with some device optimization.

Acknowledgments

Authors deeply thank Hamamatsu Photonics K.K. for providing SOI-CMOS devices. This work was supported by the JST-CREST (JPMJCR15Q7), the Cooperative Research Project of the Research Center for Biomedical Engineering with RIE, Shizuoka University, and the Cooperative Research Project Program of RIEC, Tohoku University.

References

- 1) P. Martyniuk, J. Antoszewski, M. Martyniuk, L. Faraone, and A. Rogalski, *Appl. Phys. Rev.* **1**, 041102 (2014).
- 2) K. Yamamoto, M. Yamaguchi, F. Miyamaru, M. Tani, M. Hangyo, *J. Appl. Phys.* **43 (3B)**, (2004) L414.
- 3) K. Kawase, Y. Ogawa, Y. Watanabe, H. Inoue, *Opt. Express* **11** (20) (2003) p. 2549.
- 4) Y. Nemirovsky, A. Svetlitz, I. Brouk, S. Stolyarova, *IEEE Trans. Electron Devices.* **60** (2013) p. 1575–1583.
- 5) L. E. Garn, *J. Appl. Phys.* **55** (1984) p. 1243–1253.
- 6) P. W. Kruse, *Uncooled Thermal Imaging. Arrays, Systems, and Applications.* (Bellingham, WA, USA: SPIE), (2001).
- 7) D. P. Neikirk, W.W. Lam, D.B. Rutledge, **5** (1984) p. 245–278.
- 8) S. Chen, H. Ma, S. Xiang, X. Yi, *Smart Mater. Struct.* **16** (2007) p. 696–700.
- 9) C. Chen, X. Yi, X. Zhao, B. Xiong, *Sens. Actuators A* **90** (2001) p. 2000–2002.
- 10) C. Chen, X. Yi, J. Zhang, X. Zhao, *Infrared Phys. Technol.* **42** (2001) p. 87–90.
- 11) H. Wang, X. Yi, G. Huang, J. Xiao, X. Li, S. Chen, *Infrared Phys. Technol.* **45** (2004) p. 53–57.
- 12) R.K. Bhan, R.S. Saxena, C.R. Jalwania, S.K. Lomash, *Def. Sci. J.* **59** (2009) p. 580–589.
- 13) H. K. Lee, J. B. Yoon, E. Yoon, S. B. Ju, Y. J. Yong, W. Lee, S. G. Kim, *IEEE Trans. Electron Devices.* **46** (1999) p. 1489–1491.
- 14) A. Banerjee, H. Satoh, Y. Sharma, N. Hiromoto, and H. Inokawa, *Sens. Actuators A* **273** (2018) p. 49-57.
- 15) F. Niklaus, E. Kälvesten, G. Stemme, *J. Micromechanics Microengineering.* **11** (2001) p. 509–513.
- 16) F. Niklaus, J. Pejnefors, M. Dainese, M. Haggblad, P.-E. Hellstrom, U.J. Wallgren, G. Stemme, *Proc. SPIE* **5406** (2004) p. 521.
- 17) M. Ueno, Y. Kosasayama, T. Sugino, Y. Nakaki, Y. Fujii, H. Inoue, K. Kama, T. Seto, M. Takeda, M. Kimata, *Proc. SPIE* **5783** (2005) p. 566-577.
- 18) L. Gitelman, S. Stolyarova, S. Bar-Lev, Z. Gutman, Y. Ochana, Y. Nemirovsky, *IEEE Trans. Electron Devices.* **56** (2009) p. 1935–1942.
- 19) D.S. Tezcan, S. Eminoglu, T. Akin, *IEEE Trans. Electron Devices.* **50** (2003) p. 494–502.

- 20) F. Simoens, J. Meilhan, J.A. Nicolas, J. Infrared, Millimeter, Terahertz Waves. **36** (2015) p. 961–985.
- 21) T. Ishikawa, M. Ueno, Y. Nakaki, K. Endo, Y. Ohta, J. Nakanishi, Y. Kosasayama, H. Yagi, T. Sone, M. Kimata, Proc. SPIE **4130** (2000) p. 152.
- 22) M. Kimata, M. Ueno, M. Takeda, T. Seto, Proc. SPIE **6127** (2006) p. 61270X.
- 23) Z. Olgun, O. Akar, H. Kulah, T. Akin, Proc. Int. Solid State Sensors and Actuators Conf. (Transducers '97), Chicago, IL, USA, 1997, pp. 1263-1266 vol.2.
- 24) A. Varpula, A. V Timofeev, A. Shchepetov, K. Grigoras, J. Hassel, J. Ahopelto, M. Ylilammi, M. Prunnila, Appl. Phys. Lett. **110** (2017) 262101.
- 25) M. Strasser, R. Aigner, C. Lauterbch, T.F. Sturm, M. Franosch, G. Wachutka, Sens. Actuators A **114** (2004) 362.
- 26) A. Stranz, J. Kähler, A. Waag, E. Peiner, J. Electron. Mater. **42** (2013) p. 2381–2387.
- 27) P. G. Klemens, Int. J. Thermophys. **15** (1994) p. 1345-1351.
- 28) S. Uma, A. D. McConnell, M. Asheghi, K. Kurabayashi, K. E. Goodson, Int. J. Thermophys. **22** (2001) p. 605-616.
- 29) D. Elamaram, H. Satoh, N. Hiromoto and H. Inokawa, 31st Int. Microprocesses and Nanotech. Conf. Sapporo, Japan, (2018) 15p-7-28.
- 30) M. Aoki, M. Takeda, and N. Hiromoto, Makara Seri Teknologi, **17** (2013) 1-6.
- 31) S. Zhang, Y. Yang, S.M. Sadeghipour, M. Asheghi, Proc. of HT2003 ASME Summer Heat Transfer. Conf. Las Vegas, Nevada, USA (2003) p. 1–4.
- 32) Y. Yang, R.M. White, M. Asheghi, J. Heat Transfer. **128** (2006) p. 113.
- 33) W. E. Beadle, J. C. C. Tsai and R. D. Plummer, *Quick Reference Manual of Semiconductor Engineers* (Wiley, New York, 1985) pp. 2-20~2-41.
- 34) O. Yamashita and N. Sadatomi, Jpn. J. Appl. Phys. **38** (1999) 6394.
- 35) Y. Ohishi, J. Xie, Y. Miyazaki, Y. Aikebaier, H. Muta, K. Kurosaki, S. Yamanaka, N. Uchida, and T. Tada, Jpn. J. Appl. Phys. **54** (2015) p. 071301.
- 36) J. Kim, Y. Hyun, Y. Park, W. Choi, S. Kim, H. Jeon, T. Zyung, and M. Jang, J. Nanosci. Nanotechnol. **13** (2013) p. 6416-6419.
- 37) A. Van Herwaarden, S. Van Herwaarden, Sensors Mater. **8** (1996) p. 373–387.

- 38) J. H. Kim, J. J. Kim, K. O. Lee, C. E. Lee, J. H. Lee, D. S. Kim, N. J. Kim and K. D. Yoo, 2012 IEEE 12th Topical Meeting on Silicon Monolithic Integrated Circuits in RF Systems, Santa Clara, CA (2012) p. 121-124.
- 39) D. Elamaran, H. Satoh, and H. Inokawa, 78th spring meeting, Ext. Abstr. (78th Fall Meet., 2017); Japan Society of Applied Physics, 7a-A409-7.
- 40) A. Tiwari, H. Satoh, M. Aoki, M. Takeda, N. Hiromoto, H. Inokawa, International Journal of ChemTech Research, **7** (2015) p. 1019-1026.
- 41) A. I. Boukai, Y. Bunimovich, J. T.-Kheli, J. K. Yu, W. A. Goddard, and J. R. Heath, Nature, **451** (2008) p. 168-171.

Figure Captions

Fig. 1. (a) Schematic representation of fabricated bolometer structure, and (b) cross-sectional view.

Fig. 2. (a, b) OM image of the unit bolometer device with thermocouple on top of the heater (c, d) FE-SEM image of fabricated bolometer with integrated heater and thermocouple at the center.

Fig. 3. Assumed antenna-coupled bolometer structure with a half-wave dipole antenna at both ends of the heater.

Fig. 4. Measured sheet resistance and TCR of polysilicon heater for (a) Device A and (b) Device B. The sample temperature is controlled by the prober system, and the resistance at zero heater current, i.e. without heating, is estimated by extrapolating resistance vs. current squared characteristics.

Fig. 5. Analytical estimation of temperature distribution along the wire for (a) Device A and (b) Device B.

Fig. 6. (a) Estimated maximum temperature with respect to the square of input current, and (b) Thermocouple V_{out} with respect to the temperature difference. The slope is the sum of the absolute Seebeck coefficients of n^+ and p^+ Si in the unit of V/K.

Fig. 7. (a) Measured V_{out} with respect to the applied AC input power P_{in} . The slope is the responsivity (V/W). (b) Heater input vs. heater output. (c) Frequency response of the thermocouple V_{out} . (d) Measured noise voltage in the thermocouple V_{out} .

Table I. Types of fabricated thermocouple

Device	n-type	p-type
Device A	n ⁺ single crystalline Si	p ⁺ single crystalline Si
Device B	n ⁺ polysilicon	p ⁺ single crystalline Si

Table II. Comparison of reported Seebeck coefficients at around 300 K.

Type	Dopant	N (cm ⁻³)	ρ (m Ω .cm)	S (μ V/K)	Ref
n ⁺ poly cryst. Si	P	1.0×10^{20}	-	-190	34)
p ⁺ poly cryst. Si	B	2.5×10^{19}	-	375	
n ⁺ single cryst. Si	P	6.8×10^{19}	1.1	-180	35)
p ⁺ single cryst. Si	B	1.2×10^{20}	1.3	170	
n ⁺ single cryst. Si	P	1.0×10^{20}	1.1	-128	36)
p ⁺ single cryst. Si	B	1.0×10^{20}	1.2	142	
n ⁺ poly cryst. Si	P	2.5×10^{20}	0.81	-57	25)
p ⁺ poly cryst. Si	B	2.5×10^{20}	2.2	103	
n ⁺ single cryst. Si	P	4.8×10^{19}	1.9	386*	24)
p ⁺ single cryst. Si	B	7.9×10^{19}	1.8		
n ⁺ single cryst. Si	As	1.0×10^{20}	0.97	345*	This work
p ⁺ single cryst. Si	B	2.5×10^{19}	4.2		
n ⁺ poly cryst. Si	P	$> 10^{20}$	0.92	327*	
p ⁺ single cryst. Si	B	2.5×10^{19}	4.2		

*Sum of absolute Seebeck coefficients of n- and p-type materials.

Table III. Extracted thermal conductivity

Material	k (W/Km)
n ⁺ polysilicon	22.5
n ⁺ , p ⁺ single crystalline Si	27.4

k for SiO₂ assumed to be 1.38 W/Km³⁷⁾

Table IV. Comparison of thermocouple with different temperature sensors

Device	Voltage noise (at 10Hz) V/(Hz) ^{1/2}	Responsivity V/W	NEP W/(Hz) ^{1/2}
N MOSFET	1.27 x 10 ⁻⁰⁶	6.27 k	2.02 x 10 ⁻¹⁰
PN-junction diode (without body doping)	2.08 x 10 ⁻⁰⁷	146	1.42 x 10 ⁻⁰⁹
Resistive (n ⁺ single crystalline Si)	2.70 x 10 ⁻⁰⁸	5.27	5.12 x 10 ⁻⁰⁹
Resistive (n ⁺ poly Si)	1.78 x 10 ⁻⁰⁸	2.69	6.59 x 10 ⁻⁰⁹
Thermocouple (device A in this work)	2.72 x 10 ⁻⁰⁸	56.3	4.83 x 10 ⁻¹⁰
Thermocouple (device B in this work)	3.46 x 10 ⁻⁰⁸	49.3	7.02 x 10 ⁻¹⁰

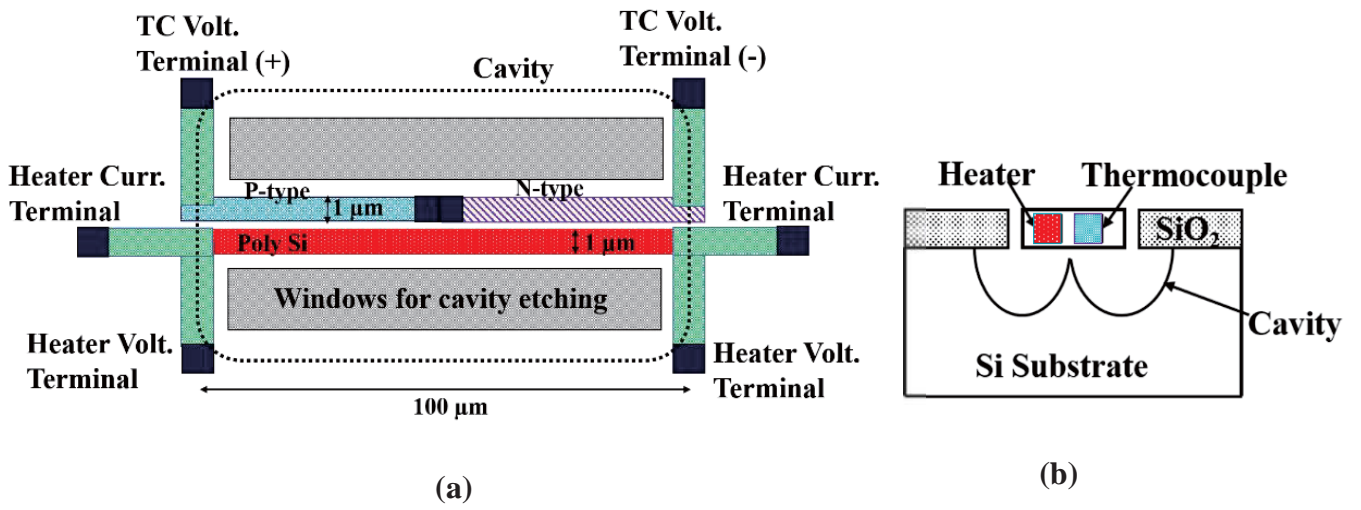


Fig.1. (a) and (b) [Color online]

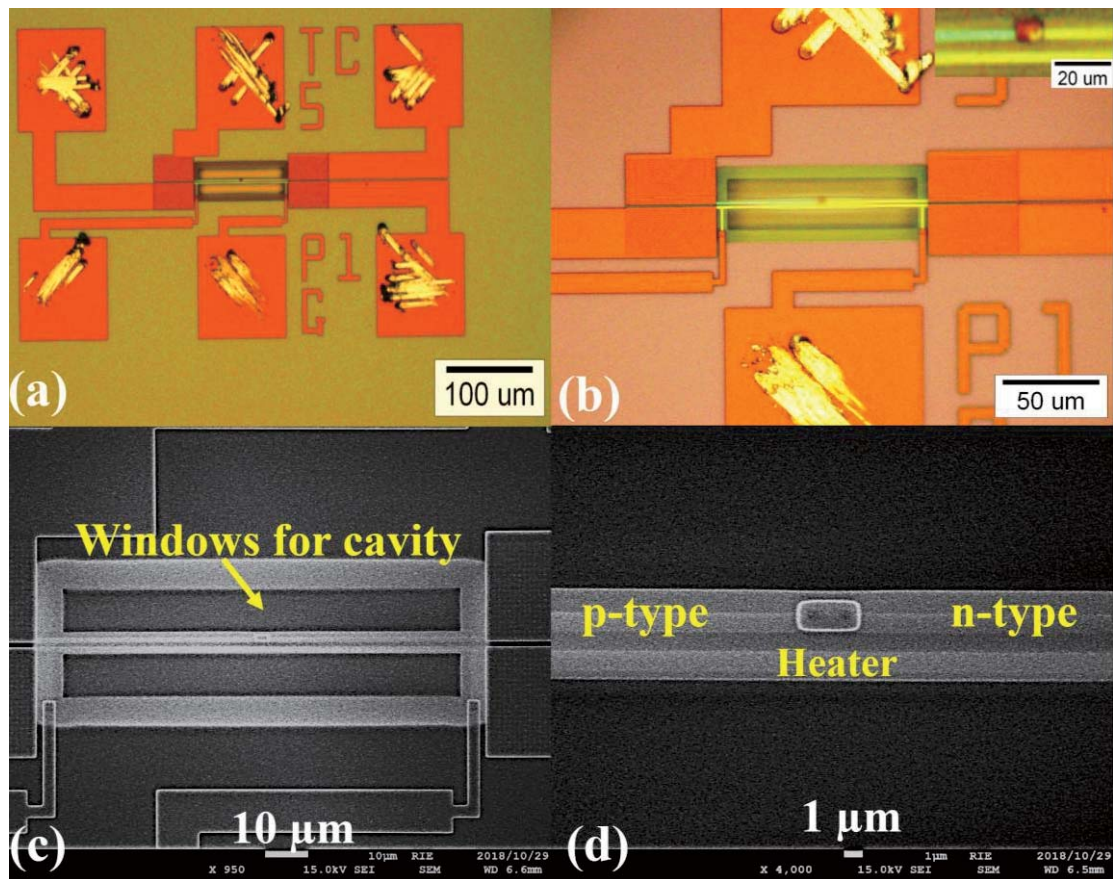


Fig. 2. [Color online]

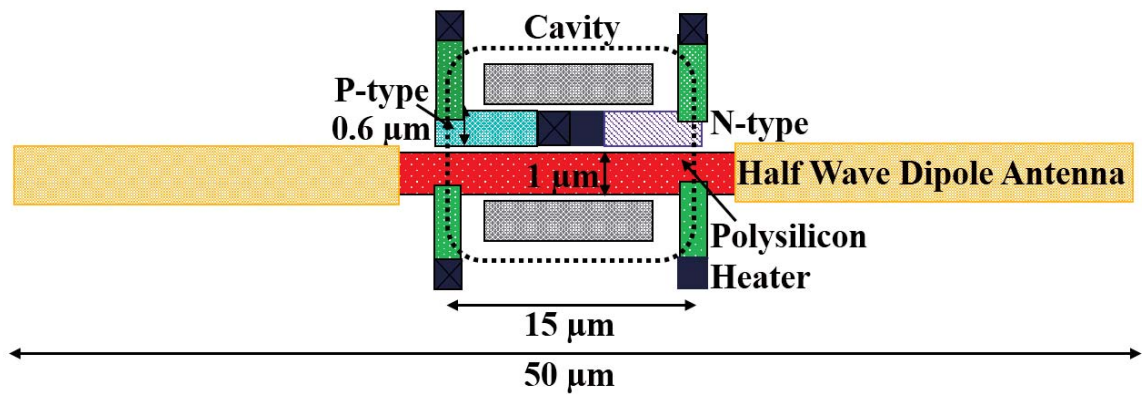


Fig. 3. [Color online]

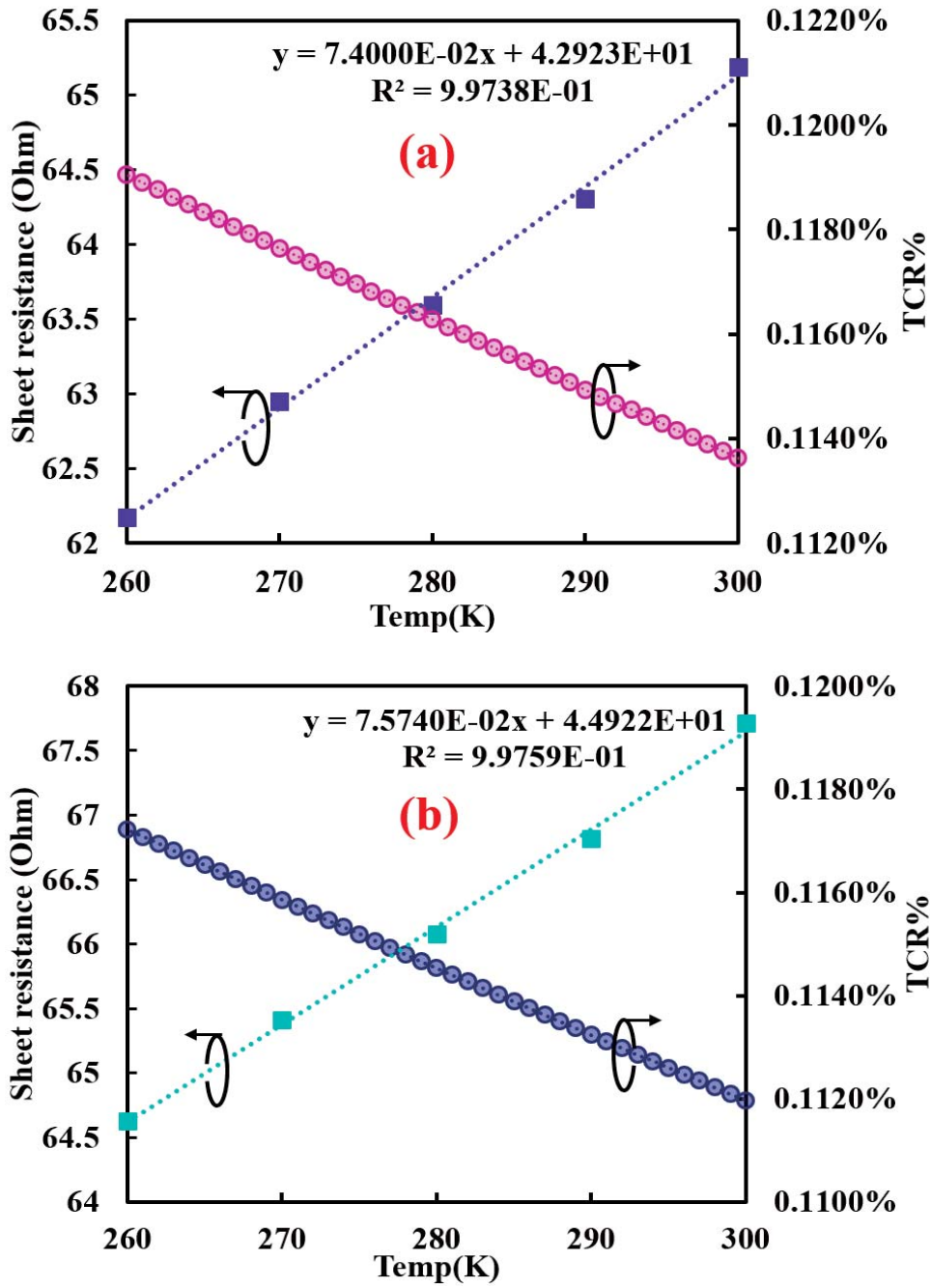


Fig. 4. [Color online]

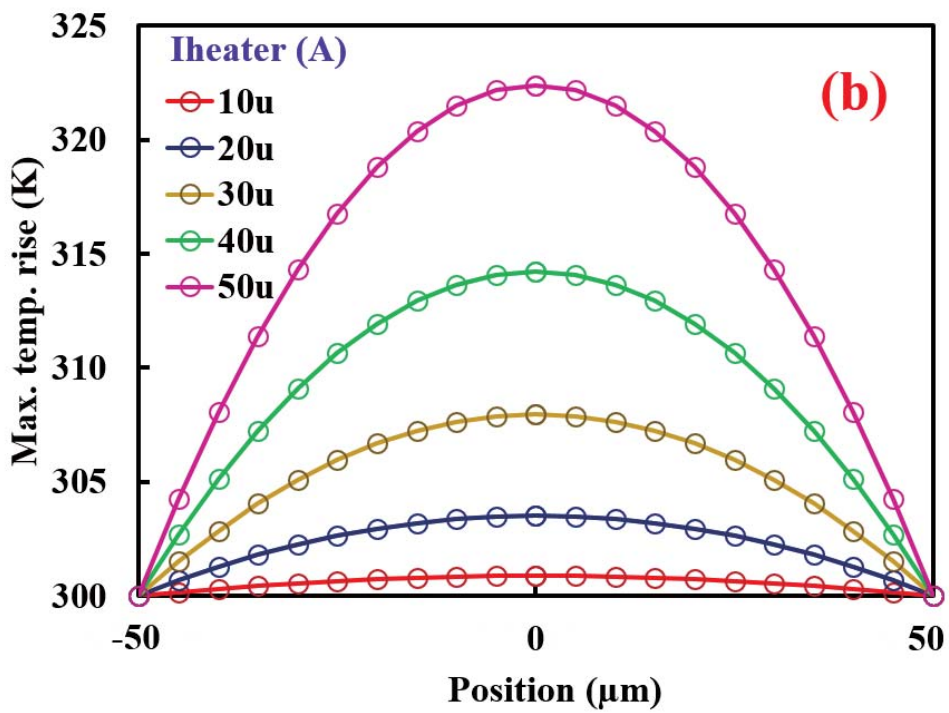
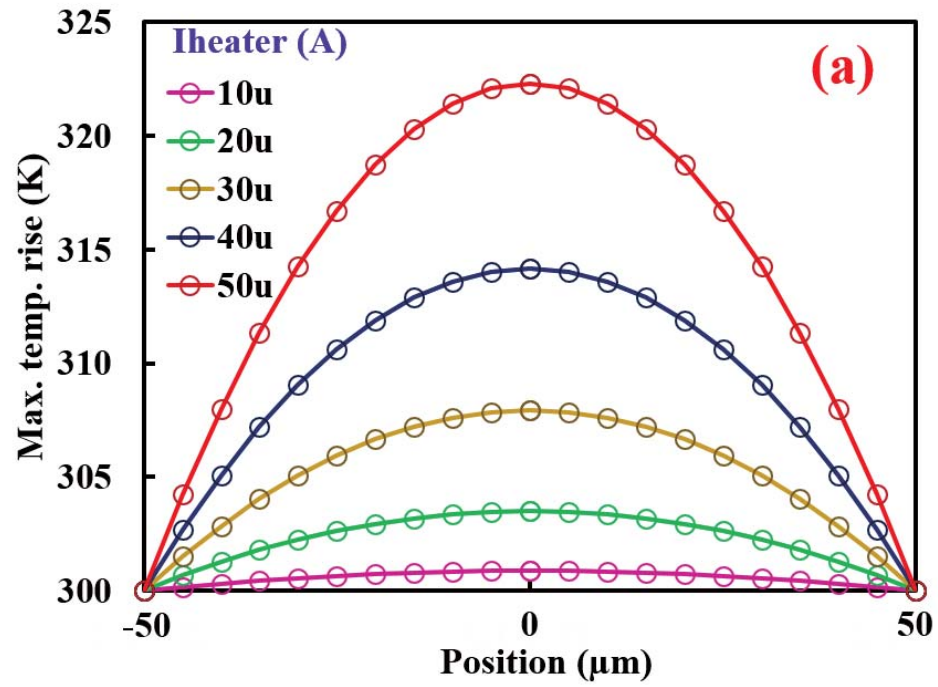


Fig. 5. [Color online]

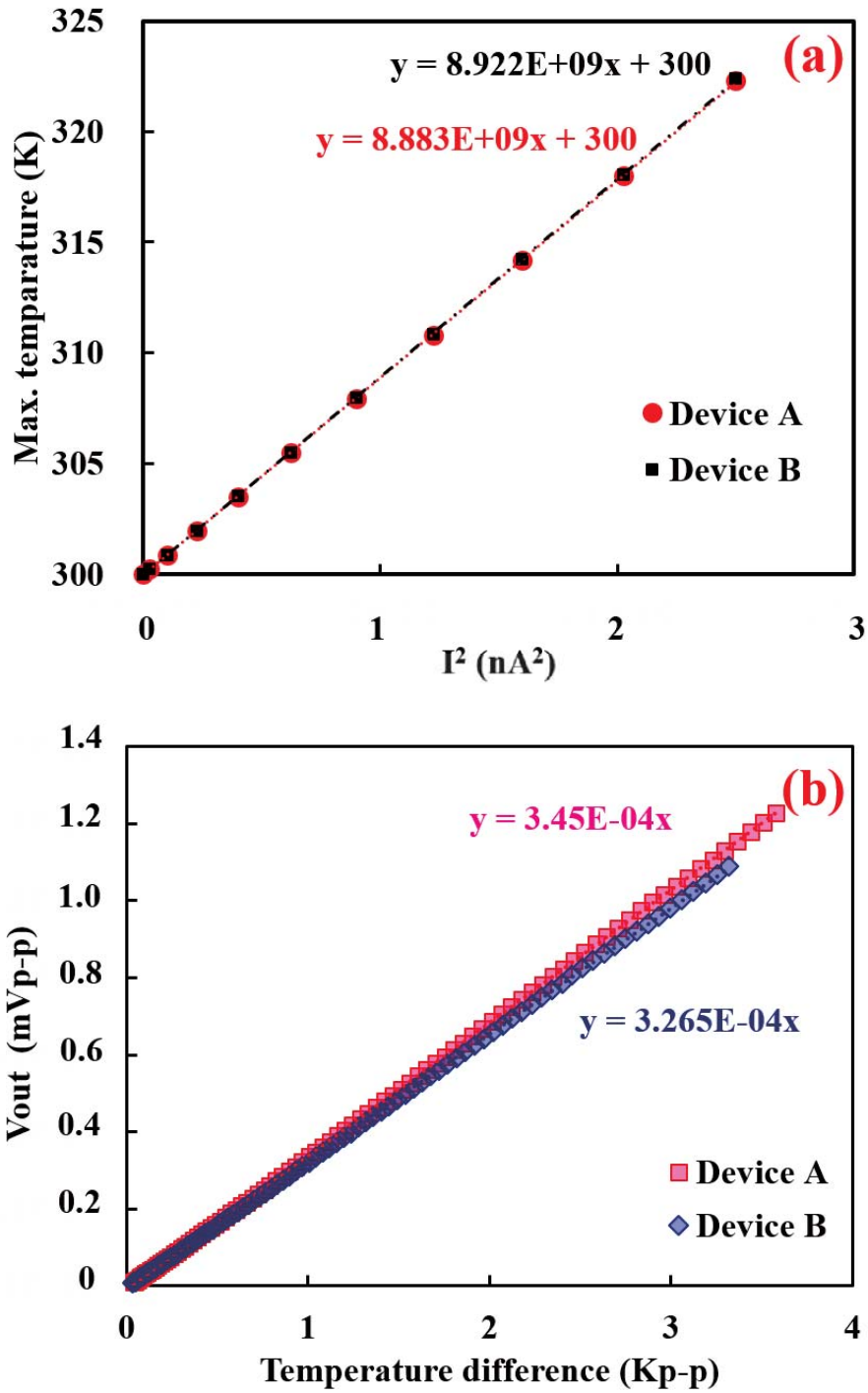


Fig. 6. [Color online]

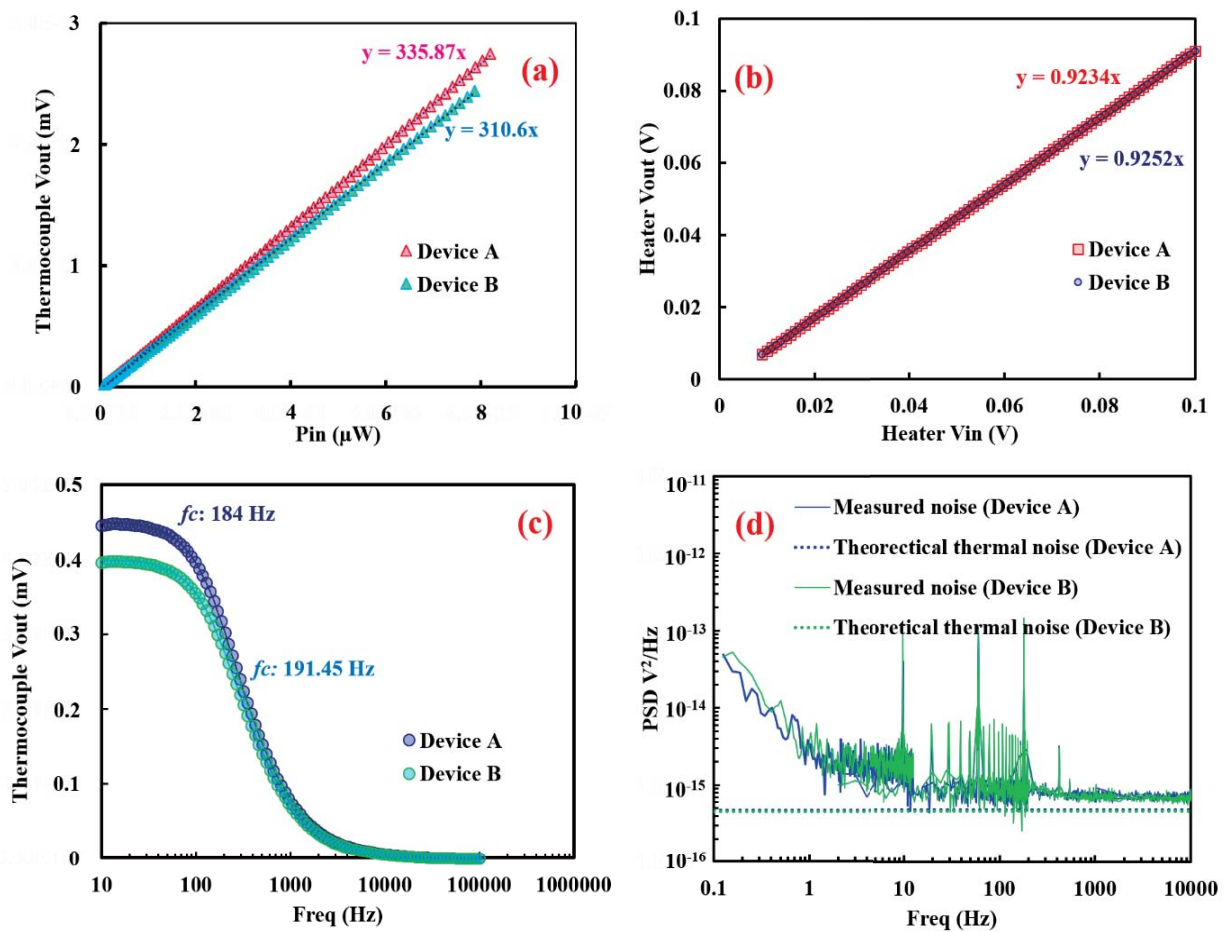


Fig. 7. [Color online]